Biosensors and Bioelectronics 194 (2021) 113633

Contents lists available at ScienceDirect

Biosensors and Bioelectronics

journal homepage: www.elsevier.com/locate/bios

Palindromic-assisted self-annealing transcription amplification for reliable genotyping of epidermal growth factor receptor exon mutations

Rui Yuan [a,b,c,1], Wanyan Tang [a,1], Hong Zhang [b,c,1], Wenxin You [a,b], Xiaolin Hu [b], Haiwei Zhang [a], Ling Chen [d], Weiqi Nian [a,**], Shijia Ding [d,***], Yang Luo [b,*]

[a] Chongqing Key Laboratory of Translational Research for Cancer Metastasis and Individualized Treatment, Chongqing University Cancer Hospital, Chongqing, 400030, PR China
[b] Center of Smart Laboratory and Molecular Medicine, School of Medicine, Chongqing University, Chongqing, 400044, PR China
[c] College of Bioengineering, Chongqing University, Chongqing, 400044, PR China
[d] Key Laboratory of Clinical Laboratory Diagnostics (Ministry of Education), College of Laboratory Medicine, Chongqing Medical University, Chongqing, 400016, PR China

ARTICLE INFO

Keywords:
Circulating tumor DNA
Isothermal amplification
Lung cancer
Molecular diagnosis
Palindromic structure

ABSTRACT

Reliable discrimination of specific epidermal growth factor receptor (EGFR) gene mutations plays a critical role in guiding lung cancer therapeutics. Until now, convenient and accurate recognition of the specific deletion of EGFR exons has remained particularly challenging. Herein, we propose a palindromic-assisted self-annealing transcription amplification (PASTA) strategy for the reliable detection of circulating EGFR exon mutations. We designed a palindromic DNA hairpin nanorobot consisting of a palindromic tail, a T7 promoter, a target recognition region, and a transcription template. The nanorobot enabled prompt self-assembly into a target-hairpin/hairpin-target dimer in the presence of single-stranded DNA target and further triggered *in vitro* transcription. In a proof-of-concept experiment for detecting circulating 15n-del EGFR mutation, a detection limit of 0.8 fM and a linear detection range of 1 fM to 100 pM was achieved, and an accuracy of 100% was reached in clinical validation by analyzing 20 samples from clinical lung cancer patients. Empowered by the intrinsic sensitivity and selectivity, the proposed PASTA approach will lead to the development of a universal platform for reliable molecular subtyping.

1. Introduction

Lung cancer has the highest morbidity and mortality among cancer-related diseases (Bade et al., 2020; Bray et al., 2018). The epidermal growth factor receptor (EGFR), as its key driver, has become a vital diagnostic and therapeutic biomarker among circulating tumor DNA (ctDNA) for early clinical intervention. (Wu and Shih (2018); Isomoto et al., 2020; Keller et al., 2020). Although it has been demonstrated that ctDNA is easier to obtain than tissue biopsy in reflecting drug response, the accuracy of the EGFR genotyping is largely limited because of its low abundance (Campos-Carrillo et al., 2019; Qiu et al., 2020; Zhu et al., 2020). Thus, it is necessary to propose new strategies with high sensitivity and selectivity to genotype EGFR mutations.

Current EGFR genotyping methods have some defects in practical applications. For instance, sequencing requires complicated library preparation process and labor-intensive bioinformatics analysis (Heider et al., 2020; Provencio et al., 2020; Wan et al., 2020); PCR-based technologies, such as digital PCR (Chen et al., 2021; Xiang et al., 2020), mutation-selected amplification-specific system PCR (Cohen et al., 2020; Zhu et al., 2019), are prone to the detection of a class of mutations; isothermal amplification strategies exemplified by DNA self-assembly (Liu et al., 2016; Wu et al., 2020), recombinase polymerase amplification (RPA) (Zhang et al., 2021), hybridization chain reaction (HCR) (Zhao et al., 2020), and CRISPR/Cas system (Gootenberg et al., 2017; Harrington et al., 2018), have been widely criticized for their low accuracy in subtype analysis, owing to the insufficient

* Corresponding author.
** Corresponding author.
*** Corresponding author.
E-mail addresses: nwqone@126.com (W. Nian), dingshijia@163.com (S. Ding), luoy@cqu.edu.cn (Y. Luo).
[1] These authors contributed equally to this work.

https://doi.org/10.1016/j.bios.2021.113633
Received 25 July 2021; Received in revised form 9 September 2021; Accepted 11 September 2021
Available online 13 September 2021

sensitivity and inappropriate primer design (Wang et al., 2017).

Recently, palindromic structure has been proposed as a novel tool to bolster the analytic sensitivity and specificity of current genotyping approaches. For example, Li et al. designed an intramolecular strand-displacement amplification by a molecular beacon with two palindromic fragments (Li et al., 2019). Karami et al. fabricated a self-assembly system using a palindromic structure (Karami et al., 2020). Most recent researches have focused on the combination of palindrome structures with enzyme recognition sites (Kim et al., 2020; Mikhailov et al., 2019; Wang et al., 2019). Although they could enhance the analytical sensitivity, such designs frequently lead to obvious defects: i) inappropriate cascade amplification leads to the generation of numerous nonspecific products; ii) multiple reaction steps increase the complexity of the experiments; and iii) the compatibility problem of follow-up reactions.

Inspired by previous work on palindrome structures, a simple and highly sensitive electrochemical sensoring approach was established, named palindromic-assisted self-annealing transcription amplification (PASTA). The specific recognition of hairpin probes by target DNA and the formation of targe-hairpin/hairpin-target dimers by self-annealing of probes are key steps that trigger subsequent transcription amplification. Through the complementary binding of the capture probes immobilized on the electrode and the detective probes added to the reaction system, these numerous single-stranded RNA transcripts can be electrochemically read out after the chromogenic reaction with methylene blue (MB). Compared with classic strand displacement amplification (Xu et al., 2020), the proposed PASTA approach has demonstrated enhanced specificity and efficiency by remarkably increasing the signal-to-noise ratio.

Deletions of exon 19 (19-del) of EGFR, which account for 44.8% of the total mutations, are regarded as attractive biomarkers for the targeted therapy of lung cancer (Kobayashi et al., 2016; Liang et al., 2020). An increasing number of studies have shown that lung cancer patients with 15n-del have longer progression-free survival than other subgroups when treated with Afatinib as the first-line monotherapy (Yu et al., 2020), suggesting that detecting 15n-del is critical for the individualized treatment of lung cancer. Therefore, we took 15n-del EGFR mutation as a model to verify the practicability of the designed genotyping strategy. The results indicated that the designed electrochemical biosensing strategy presented a simple and pragmatic platform for ultrasensitive genotyping detection.

2. Materials and methods

2.1. Materials and reagents

Klenow fragment (3′-5′exo$^-$) (KF exo$^-$), 10 × KF buffer (500 mM Tris-HCl, 50 mM $MgCl_2$, 10 mM DTT, pH 8.0), T7 RNA Polymerase, 5 × Transcription buffer (200 mM Tris-HCl, 30 mM $MgCl_2$, 50 mM DTT, 50 mM NaCl, 10 mM spermidine, pH 7.9), dNTP mixture (10 mM), NTP mixture (10 mM), and DEPC-Treated Water (DEPC) were supplied by Fermentas Inc. (Ontario, Canada); 6-Mercapto-1-hexanol (MCH) was obtained from Sigma-Aldrich (USA); Gold-view, DL20 DNA Marker, and recombinant RNase inhibitor were purchased from TaKaRa (Dalian, China). All DNA oligonucleotides were synthesized and purified by Sangon Biotechnology Co., Ltd. (Shanghai, China) with high-performance liquid chromatography (HPLC), and their corresponding sequences were included in Table S-1. The buffer solutions used in this study were as follows: Tris-HCl buffer solution (50 mM Tris-HCl, 6 mM $MgCl_2$, 10 mM NaCl, pH 7.5), and phosphate buffered solution (PBS) (Na_2HNPO_4 8 mM, NaCl 136 mM, KH_2PO_4 2 mM, KCl 2.6 mM, pH 7.2–7.4). All solutions were prepared and diluted with RNase-free water.

2.2. Apparatus

Electrochemical experiments were performed on a CHI 660E electrochemical workstation (CH Ins., Shanghai, China). Electrochemical detections were employed with a three-electrode system including a gold electrode (GE) as the working electrode, a platinum wire electrode as the auxiliary and an Ag/AgCl electrode as the reference. Gel electrophoresis analyses were photographed by ChemiDoc Imaging System (Bio-Rad, California, USA). Scanning electron microscopy (SEM) and energy dispersive X-ray spectroscopy (EDS) were conducted on SU8020 eletron microscope (HITACHI, Tokyo, Janpan).

2.3. ctDNA extraction from clinical specimens

The blood samples of lung cancer patients for 15n-del genotyping were collected from Chongqing Cancer Hospital. Circulation tumor DNA was collected with a Streck Cell-Free DNA BCT tube (Novogene, Beijing, China) and extracted with an ADx® Circulating DNA Nucleic Acid Isolation Kit (AmoyDx, Xiamen, China). The detailed operation process is presented in Supporting Information S-3.

2.4. PASTA protocol

The hairpin probe (HNP) was heated in a water bath at 95 °C for 5 min and then cooled to room temperature to ensure the formation of the hairpin structure. A 10 μL volume of an extension system containing 3 μL target DNA, 1 μM hairpin probe, 500 nM each dNTP, and 0.8 unit μL^{-1} KF exo$^-$ in KF buffer was vortexed thoroughly and incubated at 41 °C for 1 h. Then, a 20 μL transcription solution was added to fulfill the transcription amplification, specifically, 1 mM NTPs, 50 nM detection probe, 0.4 unit μL^{-1} T7 RNA polymerase, 0.8 unit μL^{-1} RNase inhibitor in transcription buffer were added and the mix was incubated at 37 °C for 2.5 h.

2.5. Sensor fabrication

After the GE was pre-treated (Supporting Information S-4), 10 μL of the resulting reaction mixture was dropped on the above prepared electrode, and the transcription products hybridized with the capture probes immobilized on the GE surface for 0.5 h at room temperature. Finally, the fabricated sensor was washed thoroughly with PBS three times and immersed in PBS containing 4 μM MB for 5 min.

2.6. Electrochemical measurement

Electrical impedance spectroscopy (EIS), square wave voltammetry (SWV) and cyclic voltammetry (CV) measurements were adopted to characterize the established electrochemical biosensor, which was carried out in 0.4 M KCl containing 0.5 mM Fe $(CN)_6^{3-/4-}$. The differential pulse voltammograms (DPV) were collected from −0.6 to 0.1 V with an amplitude of 10 mV at a 50 mV s^{-1} scan rate in PBS containing 4 μM MB.

2.7. Statistical analysis

All statistical tests were analyzed with SPSS version 20.0. One-way analysis of variance (ANOVA) was adopted for the comparison of multiple groups with a suitable *post hoc* test. $p < 0.05$ was considered statistically significant.

3. Results and discussion

3.1. Design of the PASTA strategy

The schematic of the developed PASTA approach for accurate identification of EGFR mutation is illustrated in Scheme 1. Specifically, we designed a palindromic DNA hairpin nanorobot probe (HNP) that consists of four regions: (i) a palindromic sequence (in green), (ii) a target recognition region (in orange), (iii) a T7 promoter sequence (in red), and (iv) a transcription template (in purple) (Scheme 1B, and Fig. S-1). The

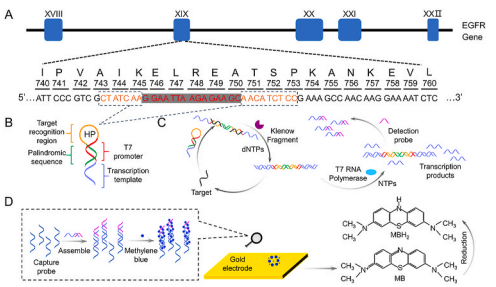

Scheme 1. The proposed PASTA strategy for genotyping EGFR mutation detection. (A) Schematic of targeted region of EGFR gene. The deleted bases are highlighted in red with a grey background. A 16 nt-long target recognition region is colored orange and boxed. Single-letter abbreviations for the amino acid residues are as follows: A, Ala; E, Glu; I, Ile; K, Lys; L, Leu; N, Asn; P, Pro; R, Arg; S, Ser; T, Thr; V, Val. (B) Design of a palindromic DNA hairpin nanorobot probe (HNP). (C) Schematic of PASTA strategy. (D) Electrochemical readout of the transcripts of the target: MB, methylene blue; MBH_2, dihydromethylene blue.

designed 16 nt-long target recognition sequence is complementary to the target 15n-del EGFR sequence, as highlighted in orange in the box in Scheme 1A. The T7 promoter sequence is composed of two sections: one can hybridize with the palindromic sequence to form the stem-loop structure of the HNP, the other section is part of a single-stranded loop structure, which ensures that a subsequent transcription is not triggered, thus avoiding any potential background signals (Wang et al., 2019).

The introduction of the target 15n-del EGFR sequence opens the stem-loop structure of the HNP, by which the palindromic sequence is released allowing them to anneal to each other and form a target-HNP/HNP-target dimer. Then the HNP extension reaction generates an HNP/HNP duplex in the presence of KF exo$^-$ and dNTPs, while the released target triggers the next cycle of the HNP extension. Additionally, with the extension of HNP, a double-stranded T7 promoter forms automatically. At this point, the exposed T7 promoter mediates the subsequent transcription amplification with the addition of T7 RNA polymerase, thus generating numerous single-stranded RNA transcripts (Scheme 1C). Finally, these RNA transcripts hybridize with the immobilized capture probes, and the residual sequence anneals the detection probes to extend the length of the duplex and increase the electrochemical signals in the presence of MB, allowing the accurate molecular mutation to be read out with a charge transfer from MB to dihydromethylene blue (MBH_2) (Scheme 1D).

3.2. Verification of the proposed strategy

We first validated the feasibility of the proposed PASTA strategy using polyacrylamide gel electrophoresis (PAGE) (Fig. 1A). Clear bands representing HNP and the target-HNP/HNP-target complex were presented in lanes 1 and 2, respectively. Lane 3 displayed an ~130 bp long extension-induced target-HNP/HNP-target dimer band. A new band with a lower molecular weight was unexpectedly observed in lane 3, indicating that the extension reaction was insufficient and that a partially completed target-HNP/HNP-target dimer existed. After the addition of T7 RNA polymerase and NTPs, a new smear band with the lowest molecular weight band of ~25 bp appeared in lane 4, illustrating the successful transcription of the target-HNP/HNP-target complex (Tan and Ng 2020). In addition, no obvious amplification products were observed in the absence of the target, indicating that there was no non-specific reaction caused by self-opening between hairpins (Fig. S-2). These results jointly confirmed the validity of the PASTA strategy.

We further validated this finding by measuring the DPV values of that target 15n-del sequence (Fig. 1B). The DPV measurements indicated that the complete PASTA procedure led to a remarkably increased oxidation peak of −0.25 V for the target 15n-del sequence in curve d (5.2 μA *vs.* 1.2 μA), indicating the existence of ample RNA transcripts (Yu et al., 2019). Notably, slight electrochemical signals were observed in the controls in the absence of either an extension or transcription reaction after the PASTA amplification, which may be caused by a weak electrostatic binding between the single-stranded DNA (capture probe) and the MB (Li et al., 2018).

The SEM with EDS mapping images of the electrode before and after modification were presented in Fig. 1C. The elemental mapping containing C (b) and O (c) were distributed on the surface of the electrode after modification. The EIS, SWV and CV measurements were employed to characterize the modification of the electrode surface in 0.4 M KCl containing 0.5 mM $Fe(CN)_6^{3-/4-}$. The semicircle diameter of the EIS curve is positively proportional to the electron transfer resistance (Ret), which was represented by the diameter of all Nyquist plots in Fig. 1D

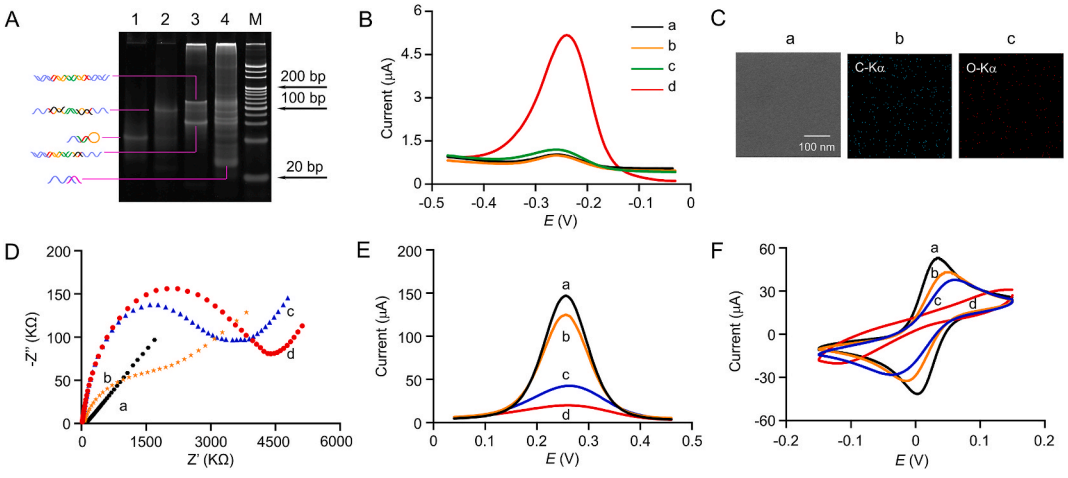

Fig. 1. Feasibility of the proposed PASTA assay for the identification of 15n-del EGFR mutation. (A) PAGE analysis of 1 μM hairpin probe (lane 1), hybridization product in the presence of 1 μM target 15n-del (lane 2), products of target 15n-del and hairpin probe after extension reaction (lane 3), transcription amplification (lane 4) and the low molecular weight ladders (lane M). (B) Typical DPV current curves of the biosensor responding to (a) blank control, (b) a target 15n-del with extension reaction only, (c) a target 15n-del with transcription reaction only, and (d) the whole PASTA procedure. (C) (a) SEM and EDS mapping images of (b) C and (c) O of the electrode before and after modification. (D) EIS, (E) SWV, and (F) CV for the (a) bare electrode, (b) electrode modified with capture probe, (c) modified with the MCH and BSA, and (d) after hybridization with transcriptional products and detection probe complex in 0.4 M KCl containing 0.5 mM Fe $(CN)_6^{3-/4-}$, respectively.

(Xue et al., 2021). The results showed that the EIS Ret was increased by ~1000 KΩ and ~1500 KΩ, respectively, after the capture probe (curve b) and MCH (curve c) were modified onto the bare GE (curve a). Meanwhile the SWV current was decreased by ~125 μA and ~42 μA, respectively, attributing to the obstruction of the electron transfer (Fig. 1D and E). The products of the RNA transcripts and detection probes subsequently yielded another increase of ~1000 KΩ for the EIS, while the peak current of SWV was decreased by an additional ~20 μA (curve d), owing to the occurrence of an electrostatic repulsion force from the negatively charged phosphate backbone of the oligonucleotides. The CV results were in good accordance with the SWV measurements (Fig. 1F). Accordingly, these results strongly suggested the successful fabrication of the proposed PASTA electrode.

3.3. Optimization of experimental parameters

To achieve the best performance of the prepared biosensor, several experimental conditions were investigated. Primarily, the concentration of KF exo$^-$ promoting the extension reaction was carefully evaluated using the peak current of DPV. As illustrated in Fig. 2A, the peak currents increased in proportion to the target concentration and reached a plateau of ~5.5 μA at the target concentration of 0.8 unit μL^{-1}. Therefore, 0.8 unit μL^{-1} KF exo$^-$ was employed for the following extension reaction. Additionally, we noticed that the peak current rose with time and reached its maximum at 2.5 h (Fig. 2B), which was subsequently set as the optimal time. We also observed that the peak current increased continually with the concentration of T7 RNA polymerase and leveled off after 0.4 unit μL^{-1}, indicating the optimal concentration of 0.4 unit μL^{-1} for the following experiments (Fig. 2C). Finally, the hybridization temperature of 25 °C and incubation time of 30 min led to a maximum signal-to-noise ratio (Fig. 2D and Fig. S-3), as the collision probability of the probes and RNA products was significantly reduced at lower temperatures, while less hybridization occurred at higher temperatures.

3.4. Analytical sensitivity of the proposed biosensor

The analytical performance of the developed PASTA biosensor was then evaluated. The results demonstrated that the DPV currents increased with the increasing concentration of the 15n-del mutation (Fig. 3A). There was a good linear correlation between the current signal and the logarithm of target ctDNA, fitted as $I = 1.541\ lgC_{15n\text{-}del} + 0.460$ with a correlation coefficient of 0.9931. Furthermore, a limit of detection (LOD) of 0.8 fM was achieved within 4 h (Fig. 3B). The LOD was calculated by the average value of negative samples plus 3 SD (95% confidence level). In contrast to previously reported detection methods, the PASTA approach achieved better performance on comprehensive analysis (Table S-2 and Table S-3). First, the palindromic-assisted signal amplification system demonstrates high amplification potential by releasing the target to trigger the next cycle in the presence of the target. Second, the partially annealed T7 promoter sequence is elaborately embedded in the stem-loop structure of HNP, thus reducing background signals by avoiding nonspecific transcription reactions in the absence of target. Third, the T7 RNA polymerase precisely recognizes the unique double-strand promoter sequence and transcribes its downstream DNA sequence at a rate of approximately 100 bp/s, thereby contributing to high transcription efficiency.

3.5. Specificity and reproducibility of the biosensor

Several other subtypes of the EGFR gene with exon 19 deletion were also analyzed using the proposed PASTA strategy to evaluate its specificity. As expected, the target DPV response of E746_A750del (15n-del) was 10-fold greater than that of the other five deletion subtypes, with only a small nucleotide difference (E746_E749del, E746_T751del, E746del, E746_S752delinsD, and E746_S752del) (Fig. 4A and B). These results strongly suggested that the proposed PASTA system possesses inherently superior selectivity, possibly due to the target-dependent extension and specific recognition of T7 RNA polymerase.

Next, we evaluated the reproducibility of this approach by detecting high and low concentrations of 15n-del samples for 20 duplicates. Similar DPV responses were observed for these duplicated tests with a relative standard deviation (RSD) less than 12.8% (Fig. 4C). Consistently, all measured values were in the interval range of $\overline{X} \pm 3\,s$ with the classical Westgard multi-rule quality control method. Thus, the PASTA system indicated acceptable reproduction (Fig. 4D).

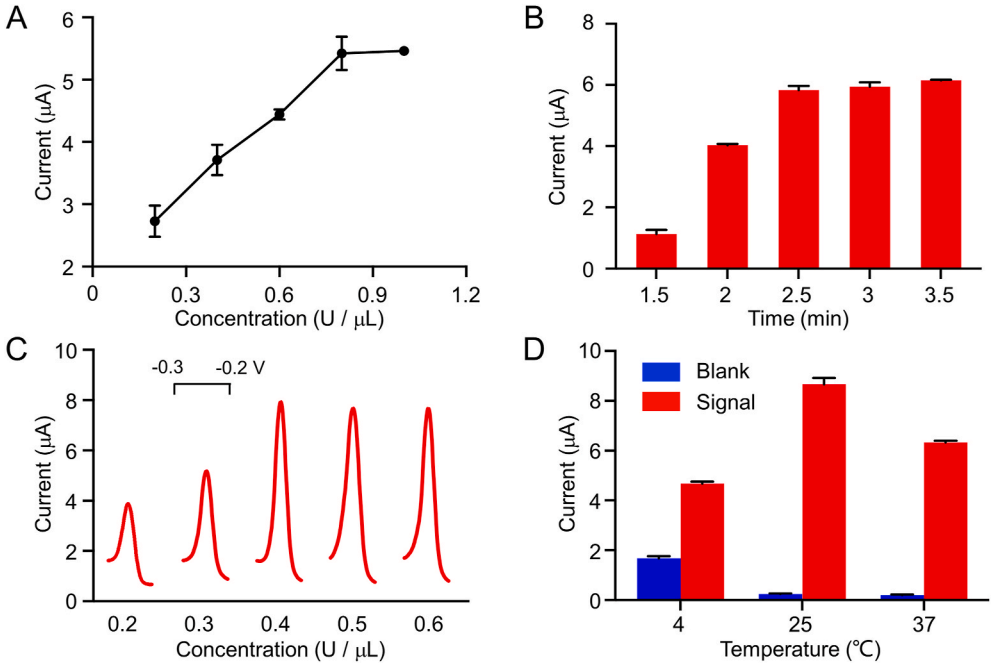

Fig. 2. Optimization of various parameters. (A) Varied KF exo$^-$ reaction concentrations for the signal response. (B) Effects of T7 RNA polymerase transcription time. (C) Concentration of the signal response; the peak of the reduction reaction is between −0.3~−0.2 V. (D) Optimized temperature for hybridization of transcription. The red column denotes positive signals and the blue column represents the blank control. Error bars represent standard derivation (n = 3). The concentration of target was 100 pM. (For interpretation of the references to color in this figure legend, the reader is referred to the Web version of this article.)

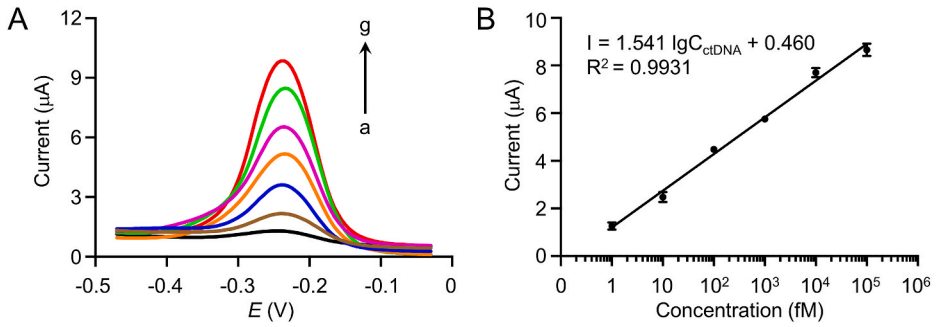

Fig. 3. Analytical performance of the PASTA strategy for 15n-del detection. (A) The DPV current curves of the proposed method responding to 0, 0.001, 0.01, 0.1, 1, 10, 100 pM of target 15n-del (from a to g). (B) The linearity between the DPV peak current and logarithmic value of target 15n-del concentrations. The error bars represent the standard deviations of three different measurements for each concentration.

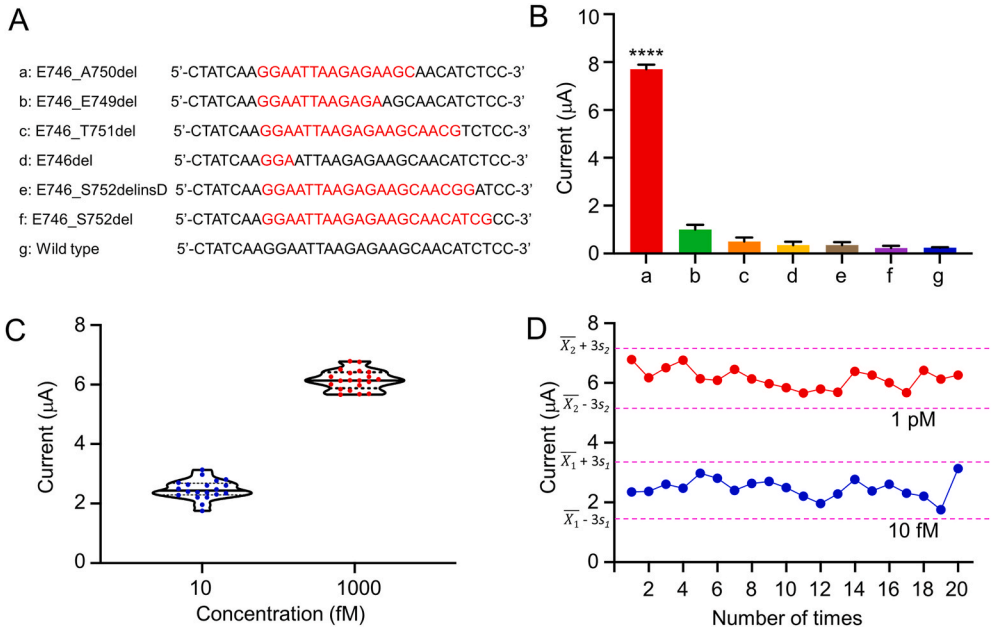

Fig. 4. Specificity and reproducibility of the PASTA strategy. (A) Sequence information. The mutated bases are highlighted in red. (B) Responses of the PASTA system to different 19-del subtypes: (a) p. E746_A750del, (b) p. E746_E749del, (c) p. E746_T751del, (d) p. E746del, (e) p. E746_S752delinsD, (f) p. E746_S752del. The data denote the means ± SEM (n = 3). ****p < 0.0001. (C) Reproducibility of the peak current among 20 replicated experiments using samples with 10 fM and 1000 fM of 15n-del mutation. (D) Levey-Jennings chart-based control for 10 fM and 1000 fM of 15n-del mutation. $\overline{X}$ represents the means of 10 fM and 1000 fM, and its corresponding standard deviation is s_1 and s_2. (For interpretation of the references to color in this figure legend, the reader is referred to the Web version of this article.)

3.6. Validation with clinical samples

To validate the analytical reliability and application potential of the developed approach, a standard addition method was adopted to analyze the 15n-del mutation in diluted serum samples from healthy volunteers. A recovery range of 86.1–106.8% was observed for different amounts of 15n-del spiked in the serum. These results suggest a low matrix effect and great potential of the proposed method for sensitive detection of 15n-del in real samples (Table S-4).

The proposed approach was then further applied to 15n-del genotyping of clinical blood samples (n = 20) from lung cancer patients after pre-amplification by PCR (Supporting Information S-8), and all test results were confirmed using commercial next-generation sequencing (NGS) assay, with 10 identified as positive and 10 as negative. This strategy was deemed positive when the detection value exceeded the threshold, i.e., the average value of negative samples plus 3 SD (95% confidence level). As shown in Fig. 5, we observed significantly higher DPV values in the mutation samples than in the threshold value (0.927 μA) from the negative samples. The receiver operating characteristic curves (ROC) indicated a high predictive power with an area under the curve (AUC) of 1.00 (95% CI: 0.89 to 1.00, p < 0.0001). Therefore, it is concluded that the developed strategy provides a promising and pragmatic tool for mutation detection in real clinical samples.

4. Conclusion

In summary, we successfully engineered a DNA nanorobot for ultrasensitive and reliable differentiation of complicated molecular mutations. This DNA nanorobot, named palindromic-assisted self-annealing transcription amplification technology, demonstrated high sensitivity in recognizing low abundance circulating EGFR 15n-del mutation with an LOD as low as 0.8 fM. The specific recognition of hairpin probes by target DNA and the formation of targe-hairpin/hairpin-target dimers by self-annealing of probes are key steps that trigger subsequent transcription amplification, after which the amplified signals could be conveniently read out using an electrochemical workstation. The proposed PASTA approach has demonstrated enhanced specificity and efficiency by remarkably increasing the signal-to-noise ratio. Both the experimental and clinical samples analyses have validated the feasibility of the PASTA method. Despite that only single molecular mutation could be recognized once in the current format, it is highly possible multiplexed detection of a series of molecular subtypes could be enabled once the microfluidic technologies are integrated. Overall, the proposed PASTA strategy presents a convenient and pragmatic platform for the accurate detection of various circulating ctDNA, laying the foundation for the development of robust tools for molecular genotyping.

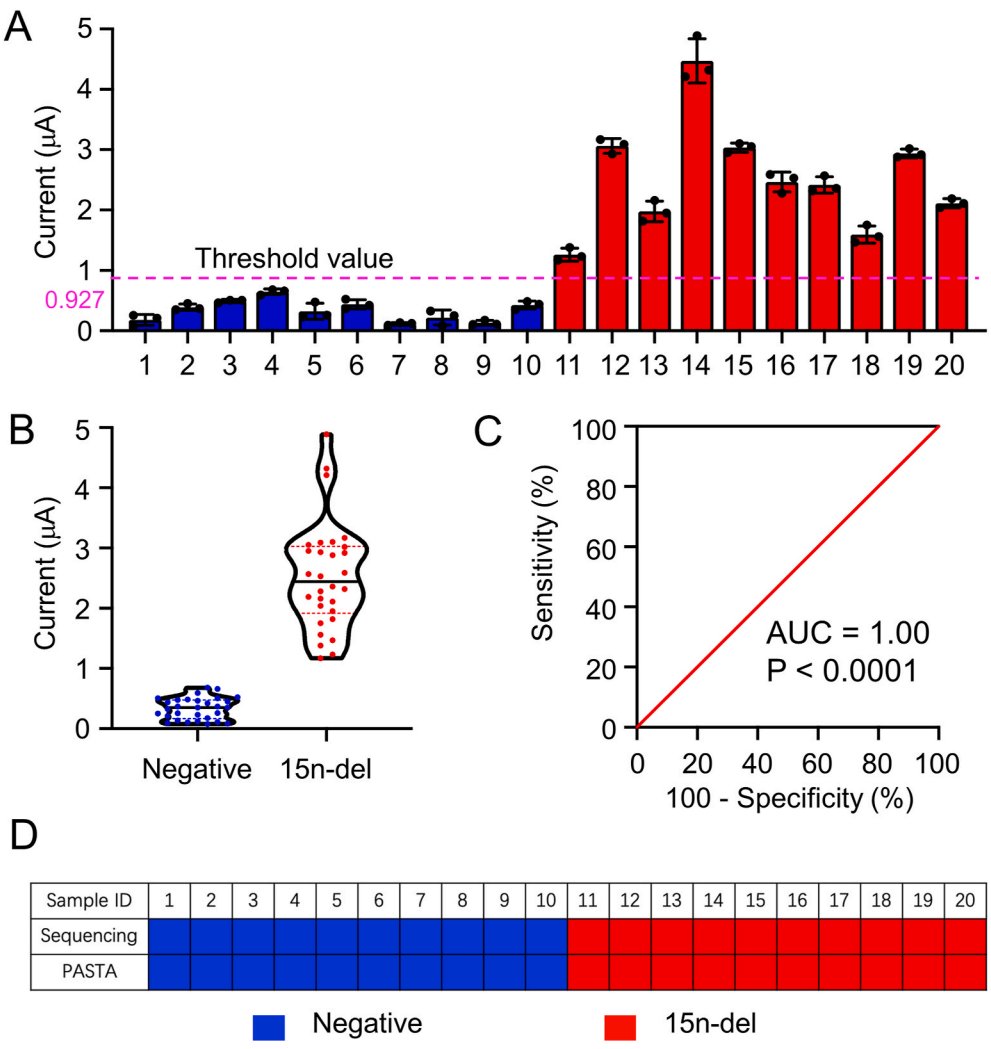

Fig. 5. Detection of 15n-del mutations in clinical samples from non-small cell lung cancer (NSCLC) patients. (A) The results of 15n-del mutation were detected by the PASTA approach in 20 samples. The noise-oriented threshold value of fluorescence intensity was defined as the average value of negative samples plus 3 SD (95% confidence level). (B) DPV signals of clinically negative samples and 15n-del mutation samples (****p < 0.0001). (C) Receiver operator characteristic (ROC) curve of 15n-del mutation versus wild type. (D) Summary of test results: blue boxes indicate that mutation was not detected in negative controls, and red boxes show that the 15n-del mutation was tested positive. (For interpretation of the references to color in this figure legend, the reader is referred to the Web version of this article.)

CRediT authorship contribution statement

Rui Yuan: Conceptualization, Methodology, Software, Writing – review & editing. **Wanyan Tang:** Methodology, Writing – review & editing. **Hong Zhang:** Software, Writing – review & editing. **Wenxin You:** Methodology, Validation. **Xiaolin Hu:** Writing – original draft, preparation. **Haiwei Zhang:** Software. **Ling Chen:** Investigation. **Weiqi Nian:** Methodology, Data curation, Validation. **Shijia Ding:** Conceptualization, Writing – review & editing, Supervision. **Yang Luo:** Conceptualization, Writing – review & editing, Supervision.

Declaration of competing interest

The authors declare that they have no known competing financial interests or personal relationships that could have appeared to influence the work reported in this paper.

Acknowledgements

This work was financially supported by the National Natural Science Foundation of China (82125022, 82072383, 81871733, and 81772061), Chongqing Research Institute Performance Incentive Guidance Special Project (cstc2018jxjl130026), Chongqing Special Postdoctoral Science Foundation (XmT2018069), the Fundamental Research Funds for the Central Universities (2019CDYGZD005 and 2019CDYGYB005), the Open Foundation of Key Laboratory of Wuliangye-flavor Liquor Solid-state Fermentation, China National Light Industry (H20200442), the Key Natural Science Foundation of Chongqing (CSTC2020JCYJ-ZDXMX0006, CSTC2020JSCX-CYLHX0001), the Key Natural Science Foundation of Chongqing Education Commission (KJZD-M202000101), Foundation of Chongqing Health Commission (2020FYYX018) and the Postgraduate Supervisor Team Funds for the Chongqing Education Commission (YDSTD1924).

Appendix A. Supplementary data

Supplementary data related to this article can be found at https://doi.org/10.1016/j.bios.2021.113633.

References

Bade, B.C., Cruz, C.S.D., 2020. Clin. Chest Med. 41, 1–24.
Bray, F., Ferlay, J., Soerjomataram, I., Siegel, R.L., Torre, L.A., Jemal, A., 2018. CA-Cancer. J. Clin. 68, 394–424.
Campos-Carrillo, A., Weitzel, J.N., Sahoo, P., Rockne, R., Mokhnatkin, J.V., Murtaza, M., Gray, S.W., Goetz, L., Goel, A., Schork, N., Slavin, T.P., 2019. Pharmacol. Therapeut. 207, 107458.
Chen, D., Wu, Y., Hoque, S., Tilley, R.D., Gooding, J.J., 2021. Chem. Sci. 12, 5196–5201.
Cohen, D., Hondelink, L.M., Solleveld-Westerink, N., Uljee, S.M., Ruano, D., Cleton-Jansen, A.M., Jan, H., Ramai, S.R.S., Postmus, P.E., van Roggen, J.F.G., Hoppe, B.P. C., Clahsen, P.C., Maas, K.W., Ahsmann, E.J.M., ten Heuvel, A., Smedts, F., van Rossem, R.N., van Wezel, T., 2020. J. Thorac. Oncol. 15, 1000–1014.
Gootenberg, J.S., Abudayyeh, O.O., Lee, J.W., Essletzbichler, P., Dy, A.J., Joung, J., Verdine, V., Donghia, N., Daringer, N.M., Freije, C.A., Myhrvold, C., Bhattacharyya, R.P., Livny, J., Regev, A., Koonin, E.V., Hung, D.T., Sabeti, P.C., Collins, J.J., Zhang, F., 2017. Science 356, 438–442.

Harrington, L.B., Burstein, D., Chen, J.S., Paez-Espino, D., Ma, E., Witte, I.P., Cofsky, J.C., Kyrpides, N.C., Banfield, J.F., Doudna, J.A., 2018. Science 362, 839–842.
Heider, K., Wan, J.C., Hall, J., Belic, J., Boyle, S., Hudecova, I., Gale, D., Cooper, W.N., Corrie, P.G., Brenton, J.D., Smith, C.G., 2020. Clin. Chem. 66, 697–705.
Isomoto, K., Haratani, K., Hayashi, H., Shimizu, S., Tomida, S., Niwa, T., Yokoyama, T., Fukuda, Y., Chiba, Y., Kato, R., Tanizaki, J., Tanaka, K., Takeda, M., Ogura, T., Ishida, T., Ito, A., Nakagawa, K., 2020. Clin. Canc. Res. 26, 2037–2046.
Karami, A., Hasani, M., 2020. Anal. Chim. Acta 1102, 119–129.
Keller, L., Belloum, Y., Wikman, H., Pantel, K., Brit, J., 2020. Cancer 1–14.
Kim, H., Nguyen, N.-P., Turner, K., Wu, S., Gujar, A.D., Luebeck, J., Liu, J., Deshpande, V., Rajkumar, U., Namburi, S., Amin, S.B., Yi, E., Menghi, F., Schulte, J. H., Henssen, A.G., Chang, H.Y., Beck, C.R., Mischel, P.S., Bafna, V., Verhaak, R.G.W., 2020. Nat. Genet. 52, 891–897.
Kobayashi, Y., Mitsudomi, T., 2016. Canc. Sci. 107, 1179–1186.
Li, H.B., Tang, Y.Q., Zhao, W.H., Wu, Z.S., Wang, S.Q., Yu, R.Q., 2019. Anal. Chim. Acta 1065, 98–106.
Li, Y.R., Chang, Y.Y., Yuan, R., Chai, Y.Q., 2018. ACS appl. Mater. Inter. 10, 25213–25218.
Liang, H.R., Li, C.C., Zhao, Y., Zhao, S., Huang, J., Cai, X.Y., Cheng, B., Xiong, S., Li, J.F., Wang, W., Zhu, C.B., Li, W.W., He, J.X., Liang, W.H., 2020. Canc. Manag. Res. 12, 8653–8662.
Liu, Y.B., Lei, T., Liu, Z.Y., Kuang, Y.B., Lyu, J.X., Wang, Q., 2016. Int. J. Mol. Sci. 17, 792.
Mikhailov, K.V., Efeykin, B.D., Panchin, A.Y., Knorre, D.A., Logacheva, M.D., Penin, A.A., Muntyan, M.S., Nikitin, M.A., Popova, O.V., Zanegina, O.N., Vyssokikh, M.Y., Spiridonov, S.E., Aleoshin, V.V., Panchin, Y.V., 2019. Nucleic Acids Res. 47, 6858–6870.
Provencio, M., Pérez-Barrios, C., Barquin, M., Calvo, V., Franco, F., Sánchez, E., Sánchez, R., Marsden, D., Sánchez, J.C., Acosta, P.M., Laza-Briviesca, Raquel, Cruz-Bermúdez, A., Romero, A., 2020. Clin. Chem. Lab. Med. 58, 306–313.
Qiu, J.H., Xu, J.X., Zhang, K., Gu, W., Nie, L.M., Wang, G.X., Luo, Y., 2020. Theranostics 10, 2374–2384.
Tan, S.I., Ng, I.S., 2020. ACS Synth. Biol. 9, 613–622.
Wan, J.C., Heider, K., Gale, D., Murphy, S., Fisher, E., Mouliere, F., Ruiz-Valdepenas, A., Santonja, A., Morris, J., Chandrananda, D., Marshal, A., Gill, A.B., Chan, P.Y., Barker, E., Young, G., Cooper, W.N., Hudecova, I., Marass, F., Mair, R., Brindle, K.M., Stewart, G.D., Abraham, J.E., Caldas, C., Rassl, D.M., Rintoul, R.C., Alifrangis, C., Middleton, M.R., Gallagher, F.A., Parkinson, C., Durrani, A., McDermott, U., Smith, C.G., Massie, C., Corrie, P.G., Rosenfeld, N., 2020. Sci. Transl. Med. 12, eaaz8084.
Wang, L., Guo, Q.M., Yu, W.J., Qiao, L.H., Zhao, M.N., Zhang, C.Z., Hu, X.M., Yang, G.H., Xiong, L.W., Lou, J.T., 2017. Lung Canc. 114, 31–37.
Wang, R.X., Zhao, X.X., Chen, X.H., Qiu, X.P., Qing, G.C., Zhang, H., Zhang, L.L., Hu, X. L., He, Z.Q., Zhong, D.D., Wang, Y., Luo, Y., 2019. Anal. Chem. 92, 2176–2185.
Wu, D., Li, B.L., Zhao, Q., Liu, Q., Wang, D., He, B., Wei, Z., Leong, D.T., Wang, G., Qian, H., 2020. Small 16, 1906975.
Wu, S.G., Shih, J.Y., Mol, 2018. Cancer 17, 1–14.
Xiang, Z., Zou, B.J., Zhang, L.X., Ma, X.P., Qi, X.M., Wei, W., Song, Q.X., Zhou, G.H., 2020. Sensor. Actuator. B Chem. 320, 128362.
Xu, H., Wu, B.T., Wang, J., Cao, H.W., Yang, J., Hao, K.X., Chen, S., Ye, S., Shen, Z.F., 2020. Talanta 215, 120897.
Xue, Y., Wang, Y., Feng, S.N., Yan, M.X., Huang, J.S., Yang, X.R., 2021. Anal. Chem. 93, 8962–8970.
Yu, S.R., Sha, H.H., Qin, X.B., Chen, Y., Li, X.Y., Shi, M.Q., Feng, J.F., 2020. Oncogene 39, 2643–2657.
Yu, Z.H., Luan, Y.N., Li, H.Y., Wang, W., Wang, X.Y., Zhang, Q., 2019. Sensor. Actuator. B Chem. 284, 73–80.
Zhang, L.T., Peng, J., Chen, J.M., Xu, L.L., Zhang, Y.L., Li, Y., Zhao, J., Xiang, L.G., Ge, Y. S., Cheng, W., 2021. Anal. Chem. 93, 5621–5628.
Zhao, Y., Feng, Y.B., Zhang, Y.B., Xia, P., Xiao, Z.H., Wang, Z.H., Yan, H.X., 2020. Anal. Chim. Acta 1130, 107–116.
Zhu, C., Zhuang, W., Chen, L., Yang, W., Ou, W.B., 2020. Transl. Lung Cancer Res. 9, 111–138.
Zhu, J.J., Zhao, Y.F., Liu, M., Gonzalez-Rivas, D., Xu, X.N., Cai, W.J., Qi, H.W., Dai, L., Wang, Z.J., Song, X., Jiang, G.N., Yang, Y., 2019. Small 15, 1805285.